Non-linear thermo-mechanical buckling approach for composite laminated marine structures.

Rafael Pacheco-Blazquez*,[1,2], Daniel Di Capua[1,2], Julio García-Espinosa[1,3] and Ovidi Casals[4]

[1]Centre Internacional de Mètodes Numèrics a l'Enginyeria (CIMNE)
Edifici C1, Campus Norte, UPC, Gran Capitán s/n, 08034 Barcelona, Spain
e-mail: dicapua@cimne.upc.edu, julio@cimne.upc.edu
*corresponding author: rpacheco@cimne.upc.edu

[2]Departament de Resistència de Materials i Estructures a l'Enginyeria (RMEE)
Universitat Politècnica de Catalunya (UPC)
Campus Diagonal Besòs, 08019 Barcelona, Spain

[3]Escuela Técnica Superior de Ingenieros Navales (ETSIN)
Universidad Politécnica de Madrid (UPM)
Av. de la Memoria, 4, 28040 Madrid, Spain

[4]Compass Ingeniería y Sistemas S.A.
C/ Gran Capità s/n, Edifici B0, Campus Nord UPC, 08034 Barcelona, Spain
e-mail: ovidi.casals@compassis.com

ABSTRACT

This paper describes the behaviour of large-length ships built using fibre-reinforced plastic composite materials under fire and large deformations. A novel methodology is proposed in order to analyse inelastic buckling and post-buckling of steel structures due to thermal loading and also extend this to the phenomenon regarded as pyrolysis that is natural in composite structures. The methodology is validated against the literature. A model of a container-ship where a fire scenario located in the engine room is used to demonstrate the methodology against a real case scenario. The section of the cargo hold closest to the engine room is structurally analysed, focusing in the integrity of the bulkhead and the supports of the TEU containers.

Keywords: Fire Safety, Fire Collapse, Buckling, Thermo-mechanical, Composites, Marine Structures

NOMENCLATURE

ρ	density $[\frac{\text{kg}}{\text{m}^3}]$
λ	eigenvalue
$\mathbf{n}$	normal
Λ	rotation matrix
l_t	thickness [m]
v	velocity $[\frac{\text{m}}{\text{s}}]$
ϕ	volume fraction
Ω	domain
k	through-thickness thermal conductivity $[\frac{\text{W}}{\text{m°C}}]$
h_{conv}	convection coefficient $[\frac{\text{W}}{\text{m}^2\text{°C}}]$
F	degradation fraction
ϵ	emissivity
h	specific enthalpy $[\frac{\text{J}}{\text{kg}}]$
q	heat flux $[\frac{\text{W}}{\text{m}^2}]$
w	mass flux $[\frac{\text{kg}}{\text{m}^2\text{s}}]$
$\dot{m}_{s\rightarrow g}$	mass flux rate $[\frac{\text{kg}}{\text{m}^2\text{s}}]$
Q	energy source $[\frac{\text{J}}{\text{kg}}]$
C_p	specific heat capacity $[\frac{\text{J}}{\text{kg°C}}]$
$\mathbf{C_T}$	specific heat matrix $[\frac{\text{W}}{\text{m}^3}]$

σ_β	Stefan-Boltzmann constant [$5.67 \cdot 10^{-8} \frac{\mathrm{W}}{\mathrm{m^2 °K^4}}$]	I	inertia [m^4]
T	temperature [°K]	d	isotropic damage index
T_{ad}	adiabatic temperature [°K]	ν	Poisson ratio
R	universal gas constant [$8.314 \frac{\mathrm{J}}{\mathrm{kmol °K}}$]	A	pre-exponential factor of the isotropic damage model
θ	fibre orientation [m^{-1}]	$\mathbf{K}$	stiffness matrix [$\frac{\mathrm{N}}{\mathrm{m}}$]
P_{cr}	critical buckling load [N]	ε	strain
l_c	characteristic length [m]	γ	engineering shear strain
β	compress-traction coefficient	σ	stress [Pa]
D	constitutive tensor [Pa]	τ	engineering shear stress [Pa]
δ	damage threshold	ς	stress weight factor
a	displacement [m]	Π	total potential strain energy
$\bar{\sigma}$	effective stress [Pa]	E	Young modulus [Pa]
$\mathbb{C}$	elastic constitutive tensor [Pa]	χ	Mourtiz and Gibson fitting parameter
$\mathbf{f}$	force vector [N]	α	thermal expansion coefficient [$°\mathrm{K}^{-1}$]
G_f	fracture energy [$\frac{\mathrm{J}}{\mathrm{m^2}}$]		

1 INTRODUCTION

Buckling collapse is a critical structural failure because when a structural member undergoes buckling, its load-bearing capacity is detrimentally decreased. This results on a redistribution of the internal stresses inside the structure to non-buckled structural members, experimenting higher stresses that they were designed for. Current regulations from classification societies prevent this mechanical failure by means of correct scantling and limiting the span length between reinforced structural members to avoid low buckling modes.

Buckling is a bifurcation phenomenon that transitions from a stable in-plane deformation state (axial) to a new in-plane plus an out-of-plane deformation state. Buckling is a non-linear geometric dominated problem and is commonly generated when an out-of-plane perturbation is applied to a structural member that operates in in-plane state.

In practise, it is very odd to have a structure to fail under pure buckling, commonly inelastic buckling is the most common failure mechanism. Plenty of reports of accidents from bulk-carriers or container-ships (Erika, Prestige, Aegean Sea, etc.) determine buckling as the origin of collapse of those marine structures, specially those involving hull-deck buckling. However, there is very little research concerning buckling of marine structures caused by fire. Bulk-carriers, Ro-Ros or container-ships present high buckling risk in the presence of fire due to its hollow shape. Thermal buckling is not rare, marine accidents such as the MS Nordlys, MSC Flaminia, Stolt Valor or Sorrento are a good example of it. Nevertheless, the majority of large length ships (over 50 m), are designed using metal materials and thus the buckling behaviour is different to the one from Fibre Reinforced Polymers (FRP).

FRP materials present better mechanical and thermal characteristics, e.g., steel presents a higher Young's modulus, lower yielding and ultimate stress or higher thermal expansion coefficient compared to FRP (Shakir Abbood et al., 2020). Regulations such as the Convention for the Safety of Life at Sea (SOLAS) introduce the concept of '*steel equivalent*' structural material, thus when comparing the material properties of FRP to its '*steel equivalent*' two aspects arise. First, composites present a lower thermal expansion, which translates in a higher critical temperature to buckle if compared to steel.

The latter is an advantage in combination with its slow conduction of heat due to having a lower conductivity. Second, the fact that the ratio between the yield or ultimate stress over the Young's modulus is significantly higher for composites, which delay the initiation of inelastic damage specially due to thermal expansion. Other key aspects are its low density that increases the cargo capacity or being able to obtain a tailored configuration to increase the inertia such as in sandwich stacking. These characteristics show an advantage in the application of FRP against steel structures when it comes to thermal inelastic buckling.

This research is part of the European H2020 project named FIBRESHIP. The project focuses on the production of knowledge and technology to build complete large-length vessels made of FRP materials. Within the project three prototype vessels were designed, the one presented here is the container-ship exposed to fire scenario.

Fire in composites is a complex phenomenon since it involves pyrolysis, a thermo-chemical decomposition process affecting the resin (Henderson et al., 1985; Mouritz et al., 2009). Pyrolysis results in the degradation of thermo-mechanical properties of the composite as a whole and its posterior structural collapse. The thermo-mechanical analysis of composites in the presence of fire in marine applications can be summarised by the work derived from Henderson et al. (Chippendale et al., 2014; Dodds et al., 2000; Gibson et al., 1995; Henderson and Wiecek, 1987; Henderson et al., 1985; Looyeh and Bettess, 1998; Lua et al., 2006) that focuses on the solution of the one-dimensional heat equation with the assumption of pyrolysis and gas generation for FRP laminate materials. The contribution of Mouritz and Gibson (Gibson et al., 1995, 2004; Mouritz and Mathys, 2000, 2001) is significant on the thermo-mechanical characterisation of the post-fire properties of composites and authors such as Asaro et al. (Asaro et al., 2009) or Tran et al. (Tran et al., 2018) have studied the effect of thermal-buckling in composites based on this.

There are different approaches to model the constitutive behaviour of composites. Most of the research involving fire uses either the orthotropic constitutive model (Green and Naghdi, 1965) which incorporates the assumptions of Reuss (Reuss, 1929) and Voigt (Voigt, 1889). Alternatively, finer approaches are used based on the classical mixtures theory (CMT). One of this approaches is the so-called Rule of Mixtures (ROM) (Car et al., 2000; Rastellini et al., 2008) and in this particular research the Serial/Parallel Rule of Mixtures (SPROM) (Rastellini et al., 2008) has been employed, however it was adapted in order to introduce the thermal expansion of the composite.

Commonly the buckling analysis of FRP structures is performed based on linear buckling of orthotropic constitutive materials (Abdoun et al.; Al-Waily, 2015; Ounis et al., 2014; Shiau et al., 2010; Thangaratnam et al., 1989), however this would limit the calculus to linear analysis. Instead a novel thermo-mechanical model is proposed using the adapted SPROM theory and the corotational method proposed by Felippa and Haugen (Felippa and Haugen, 2005) that deals with both non-linear constitutive and geometric aspects of composite thermal buckling.

Hence this paper focuses in the development of a thermo-mechanical model for composite materials with pyrolysis. The model combines the ideas of Henderson et al. and is coupled with the non-linear geometric and non-linear constitutive mechanical model by combination of both SPROM and corotational theories. This allows to analyse composites and buckling and to take all the non-linearities of such complex problem (damage, orthotropy, pyrolysis, buckling instability, etc.). The application of this model is tested against analytical benchmark results for the Euler-buckling beam and the Laminate-plate buckling, the first case is used to illustrate the non-linear capabilities of the constitutive models and the second the usefulness of SPROM model to obtain the orthotropy, characteristically, of laminate composites. The last application is ambiented on marine structures, most of the thermal buckling applications present in literature revolve around piping, tank storage or supporting framing structures under fire loads (200, 2009; Holmas and Amdahl). The case presented here is based on a fire scenario of the machinery room in a container-ship built entirely of composite materials and how

thermal buckling plays a major role to the collapse of the structure.

2 THERMAL MODEL

The thermal model combines the governing model proposed by Henderson et al. (Henderson et al., 1985) and the flux boundary conditions are prescribed using the definition of adiabatic temperature introduced by Wickstrom Ulf et al. (Wickstrom Ulf et al., 2007)

$$\begin{cases} \rho C_p \dfrac{\partial T}{\partial t} = \nabla \cdot (k \nabla T) - \mathbf{w_g} C_{p_g} \nabla T - \dfrac{\partial \rho}{\partial t}(Q_p + h_s - h_g) & \forall x \in \Omega, t \geq 0 \\ q = (-k \boldsymbol{\nabla} \mathbf{T}) \cdot \mathbf{n} = \left(\sigma_\beta \epsilon (T_{ad_k}^4 - T_k^4) + h_{conv}(T_{ad} - T) \right) & \forall x \text{ on } \partial\Omega, t \geq 0 \\ \rho(t=0) = \rho_0 & \forall x \in \Omega \\ T(t=0) = T_0 & \forall x \in \Omega \end{cases} \tag{1}$$

where C_p is the specific heat capacity, T is the temperature, k is the through-thickness thermal conductivity, h_g is the gas specific enthalpy, $\mathbf{w_g}$ is the gas mass flux, C_{p_g} is the gas specific heat capacity, Q_p is the polymer degradation energy source, h_s is the solid specific enthalpy, q is the normal heat flux component, $\mathbf{n}$ is the normal, σ_β is the Stefan-Boltzmann constant, ϵ is the emissivity, T_{adk} is the adiabatic prescribed temperature in Kelvin, T_{ad} is the adiabatic prescribed temperature in Celsius, h_{conv} is the convection coefficient, Ω is the total domain and $\partial\Omega$ refers to the domain boundary.

In this paper the profile of temperature through-thickness is assumed to be linear if stationary regime is reached and not substantial pyrolysis has occurred (Equation 1).

$$\Delta T = \Delta T_0 + \frac{\delta T}{l_t} z \equiv \frac{T_1 + T_2}{2} + \frac{T_2 - T_1}{l_t} z \tag{2}$$

where T_1 and T_2 are the temperature of the cold and hot end respectively (see Figure 1 and Figure 7). This linear distribution is obtained when considering that the thermal properties of the different layers are the same, otherwise a stepwise linear distribution would be obtained.

3 MECHANICAL MODEL

The mechanical part of the thermomechanical model presented in this work is based in non-linear shell finite elements. The geometrical non-linear strategy is based in the corotational method developed by Felippa and Haugen. The core element used by the corotational shell model is a 3-node triangular element with three translations and three rotations per node, which is obtained by the combination of a membrane element and a plate element. The membrane element is based in the optimal triangle element with drilling rotation presented in (Felippa, 2003). The plate element is based in the classical DKT element initially presented in (Dhatt, 1970). The constitutive formulation is introduced using the Serial/Parallel Rule of Mixtures (SPROM) (Rastellini et al., 2008).

3.1 Non-linear geometric DKT element

The discrete Kirchhoff triangle presents a kinematic expressed in Voigt notation such as

$$\boldsymbol{\varepsilon} = [\varepsilon_x, \varepsilon_y, \gamma_{xy}]^T, \quad \boldsymbol{\sigma} = [\sigma_x, \sigma_y, \tau_{xy}]^T \tag{3}$$

Using the same procedure as in (Oñate, 2013), the strain can be re-written in membrane and bending components

$$\boldsymbol{\varepsilon} = \begin{bmatrix} \varepsilon_x \\ \varepsilon_y \\ \gamma_{xy} \end{bmatrix} = \begin{bmatrix} \dfrac{\partial a_x}{\partial x} \\ \dfrac{\partial a_y}{\partial y} \\ \dfrac{\partial a_x}{\partial y} + \dfrac{\partial a_y}{\partial x} \end{bmatrix} \equiv \begin{bmatrix} 1 & 0 & 0 & -z & 0 & 0 \\ 0 & 1 & 0 & 0 & -z & 0 \\ 0 & 0 & 1 & 0 & 0 & -z \end{bmatrix} \begin{bmatrix} \boldsymbol{\varepsilon_m} \\ \boldsymbol{\varepsilon_b} \end{bmatrix} \tag{4}$$

where $\mathbf{a}$ is the displacement, $\boldsymbol{\sigma}$ is the stress and $\boldsymbol{\varepsilon}$ is the strain vectors respectively. On the other hand, $\boldsymbol{\varepsilon_m}$ is the membrane strain and $\boldsymbol{\varepsilon_b}$ is the bending strain . Equation 3 and Equation 4 are expressed in local coordinate system, generally a rotation matrix ($\boldsymbol{\Lambda}$) is used to transform the local magnitudes to global. In the corotational formulation proposed by Felippa and Haugen this transformation matrix depends on the node displacements ($\mathbf{a}$).

This way the non-linear geometric dependency is introduced into the problem. Commonly the total potential strain energy is minimised with respect the displacement field (Thangaratnam et al., 1989), leading to the following buckling problem

$$\begin{cases} \dfrac{\partial \Pi}{\partial a} = \sum_{e=1}^{n_{\text{elem}}} \boldsymbol{\Lambda} \mathbf{f_i} - \mathbf{f_{ext}} = \sum_{e=1}^{n_{\text{elem}}} \boldsymbol{\Lambda}^T \mathbf{K} \boldsymbol{\Lambda} \mathbf{a} - \mathbf{f_{ext}} = 0 \\ \dfrac{\partial^2 \Pi}{\partial a^2} = |\mathbf{K}_L + \lambda \mathbf{K}_{NL}| = \boldsymbol{\Lambda} \dfrac{\partial \mathbf{f_i}}{\partial \mathbf{a}} + \dfrac{\partial \boldsymbol{\Lambda}}{\partial \mathbf{a}} \mathbf{f_i} = \boldsymbol{\Lambda}^T \mathbf{K} \boldsymbol{\Lambda} + \left(\dfrac{\partial \boldsymbol{\Lambda}^T}{\partial \mathbf{a}} \mathbf{K} \boldsymbol{\Lambda} + \boldsymbol{\Lambda}^T \mathbf{K} \dfrac{\partial \boldsymbol{\Lambda}}{\partial \mathbf{a}} \right) \mathbf{a} = 0 \end{cases} \tag{5}$$

where Π is the total potential strain energy, $\mathbf{K}$ is the stiffness matrix, $\mathbf{K}_L$ is the linear geometric stiffness matrix, $\mathbf{K}_{NL}$ is the non-linear geometric stiffness matrix , $\mathbf{f_i}$ and $\mathbf{f_{ext}}$ are the internal and external force vectors respectively. The subscript e refers to element and λ is the eigenvalue of the buckling problem.

3.2 Serial-parallel rules of mixing (SPROM)

The SPROM splits the state variables, strain and stress, into parallel and serial directions by employing the concept of projector matrices. Note that the denomination parallel and serial corresponds to the fulfilment of iso-strain and iso-stress hypothesis.

$$\boldsymbol{\varepsilon} \equiv \boldsymbol{\varepsilon_p} + \boldsymbol{\varepsilon_s} = \mathbf{P_{p,\varepsilon}} \boldsymbol{\varepsilon} + \mathbf{P_{s,\varepsilon}} \boldsymbol{\varepsilon} \tag{6}$$

$$\boldsymbol{\sigma} \equiv \boldsymbol{\sigma_p} + \boldsymbol{\sigma_s} = \mathbf{P_{p,\sigma}} \boldsymbol{\sigma} + \mathbf{P_{s,\sigma}} \boldsymbol{\sigma} \tag{7}$$

$$\text{Parallel} \quad \begin{cases} \boldsymbol{\varepsilon_p} = \boldsymbol{\varepsilon_{p,f}} = \boldsymbol{\varepsilon_{p,m}} \\ \boldsymbol{\sigma_p} = \phi_f \boldsymbol{\sigma_{p,f}} + \phi_m \boldsymbol{\sigma_{p,m}} \end{cases} \tag{8}$$

$$\text{Serial} \quad \begin{cases} \boldsymbol{\sigma_s} = \boldsymbol{\sigma_{s,f}} = \boldsymbol{\sigma_{s,m}} \\ \boldsymbol{\varepsilon_s} = \phi_f \boldsymbol{\varepsilon_{p,f}} + \phi_m \boldsymbol{\varepsilon_{p,m}} \end{cases} \tag{9}$$

where $\boldsymbol{\sigma_{p,m}}$ is the parallel matrix stress, $\boldsymbol{\sigma_{s,m}}$ is the serial matrix stress, $\boldsymbol{\sigma_{p,f}}$ is the parallel fibre stress, $\boldsymbol{\sigma_{s,f}}$ is the serial fibre stress, $\boldsymbol{\sigma_s}$ is the serial composite stress, $\boldsymbol{\sigma_p}$ is the parallel composite stress, $\boldsymbol{\varepsilon_{p,m}}$ is the parallel matrix strain, $\boldsymbol{\varepsilon_{s,m}}$ is the serial matrix strain, $\boldsymbol{\varepsilon_{p,f}}$ is the parallel fibre strain, $\boldsymbol{\varepsilon_{s,f}}$ is the serial fibre strain, $\boldsymbol{\phi_m}$ is the matrix volume fraction and $\boldsymbol{\phi_f}$ is the fibre volume fraction.

3.3 Thermal constitutive model of the constituent materials

The non-linear constitutive model used to model inelastic composites is the so-called isotropic damage model (Chaves, 2013).

$$\boldsymbol{\sigma_i} := (1 - d_i) \mathbb{C}_\mathbf{i} (\boldsymbol{\varepsilon_i} - \boldsymbol{\varepsilon_{T,i}}), \quad \forall i \in f, m \tag{10}$$

where σ_i is the stress, ε_i is the strain, d_i is the isotropic damage index, $\mathbb{C}_i$ is the elastic constitutive tensor and $\varepsilon_{T,i}$ is the thermal strain for the constituent material 'i' (fibre or matrix). The thermal strain of each of the constituent materials is anisotropic

$$\boldsymbol{\varepsilon_{T,i}} := \boldsymbol{\alpha_i}\Delta T = \boldsymbol{\alpha_i}\big(T(x,t) - T(x,0)\big), \quad \forall i \in f,m \tag{11}$$

where α_i is the thermal expansion coefficient and is defined as $\boldsymbol{\alpha} := [\alpha_x, \alpha_y, 0, 0, 0]^T$. The Kirchhoff-Love theory expresses the elastic constitutive matrix as

$$\mathbb{C}_\mathbf{i} := \frac{E_i}{1-\nu_i^2}\begin{bmatrix} 1 & \nu_i & 0 \\ \nu_i & 1 & 0 \\ 0 & 0 & \dfrac{1-\nu_i}{2} \end{bmatrix}, \quad \forall i \in f,m \tag{12}$$

where E_i is the Young modulus and ν_i is the Poisson ratio . When the composite pyrolyse, both Young's modulus (E) and yield stress (σ_y) are decreased as stated by (Mouritz and Gibson, 2006).

$$P_i(T,F) = \left(\frac{P_{u,i}+P_{r,i}}{2} - \frac{P_{u,i}-P_{r,i}}{2}\tanh\chi_{1,i}(T-T_{g,i})F^{\chi_{2,i}}\right), \quad \forall i \in f,m \tag{13}$$

where (P_u) is the unrelaxed and (P_r) is the relaxed value of a generic property (P), $T_{g,i}$ is the glass transition temperature, $\chi_{1,i}$ is the first Mourtiz and Gibson fitting parameter, $\chi_{2,i}$ is the second Mourtiz and Gibson fitting parameter.

Two changes have to be done for isotropic damage model from (Chaves, 2013) in order to take the effect of the thermal stress in the evolution of the yielding surface

$$\begin{cases} \delta_i = \left(\varsigma + \dfrac{1-\varsigma}{\beta_i}\right)\sqrt{E_{0,i}}\sqrt{\dfrac{\bar{\boldsymbol{\sigma}}_\mathbf{i}}{\sigma_{y,i}} : (\mathbb{C}_{\mathbf{0,i}})^{-1} : \dfrac{\bar{\boldsymbol{\sigma}}_\mathbf{i}}{\sigma_{y,i}}} & \forall i \in f,m \\ A_i = \left(\dfrac{G_{f_i}E_i}{l_{c,i}\,\sigma_{y,i}^2} - \dfrac{1}{2}\right) \rightarrow \dfrac{G_{f_i}E_i}{\sigma_{y,i}^2} = \text{constant} & \forall i \in f,m \end{cases} \tag{14}$$

where $\bar{\sigma}_i$ is the effective stress, δ_i is the damage threshold, ς is the stress weight factor, $\beta_{,i}$ is the compress-traction coefficient, $E_{0,i}$ is the initial Young modulus, $\sigma_{y,i}$ is the yield stress, which is considered to be dependent of the temperature and the degradation factor, $\mathbb{C}_{0,i}$ is the initial elastic constitutive tensor, $A_{,i}$ is the pre-exponential factor of the isotropic damage model , $l_{c,i}$ is the characteristic length and G_{f_i} is the fracture energy.

Equation 14 is modified to maintain a constant yielding surface if the rate of thermal degradation is null and that the rate of damage is considered constant.

3.4 SPROM with thermal expansion

Rastellini et al. derived an iterative algorithm to satisfy the iso-stress hypothesis of an orthotropic material. If thermal expansion is taken into account, the prediction of the increment of the serial strain for the matrix component yields

$$\boldsymbol{\Delta\varepsilon_{s,m}}|_0 = \mathbb{M} : \Big(\mathbb{C}_{\mathbf{sp,m}}\boldsymbol{\Delta\varepsilon_s} + \phi_f(\mathbb{C}_{\mathbf{sp,f}} - \mathbb{C}_{\mathbf{sp,m}})\boldsymbol{\Delta\varepsilon_p} + \phi_f\boldsymbol{\Delta\sigma_{T,m}} - \phi_f\boldsymbol{\Delta\sigma_{T,f}}\Big) \tag{15}$$

$$\mathbb{M} = \Big(\phi_f\mathbb{C}_{\mathbf{ss,m}} + \phi_m\mathbb{C}_{\mathbf{ss,f}}\Big)^{-1} \tag{16}$$

$$\boldsymbol{\Delta\sigma_{T,m}} = \mathbb{C}_{\mathbf{sp,m}}\boldsymbol{\Delta\varepsilon_{T,p,m}} + \mathbb{C}_{\mathbf{ss,m}}\boldsymbol{\Delta\varepsilon_{T,s,m}} \tag{17}$$

$$\boldsymbol{\Delta\sigma_{T,f}} = \mathbb{C}_{\mathbf{sp,f}}\boldsymbol{\Delta\varepsilon_{T,p,f}} + \mathbb{C}_{\mathbf{ss,f}}\boldsymbol{\Delta\varepsilon_{T,s,f}} \tag{18}$$

where $\Delta\ \sigma_{T,f}$ is the incremental stress of the fibre and $\Delta\ \sigma_{T,m}$ is the incremental stress of the matrix due to thermal expansion. Both terms are the addition into the new thermal SPROM formulation. $\mathbb{C}_{ij,k}$ is the projected elastic constitutive tensor in serial and parallel directions (i, j) for the fibre or matrix component (k).

4 VALIDATION OF THE NUMERICAL MODEL

Three numerical models are presented. First the euler-buckling beam case since it is a one-dimensional buckling problem, therefore the transverse effect present on composites can be neglected. A second case named Laminate-plate buckling is presented to show the correctness of the SPROM theory predicting orthotropy and the third, Thermal-buckling collapse of a container-ship, shows a real application of the methodology to assess structural collapse given a fire scenario.

4.1 Euler-buckling beam

The euler-buckling beam is a well-known problem, in this case the beam is simply supported in both extremes and the dimensions can be seen in Figure 1. The material is a symmetric sandwich composed of a first layer of glass fibre and vinylester with a volumetric fibre fraction of 60%, the second layer is a core of PVC with a density of 80 g/m^3 and the third layer is the same as the first. This problem is very useful since there is no transverse influence and the problem is highly influenced by the constitutive properties in the fibre-direction.

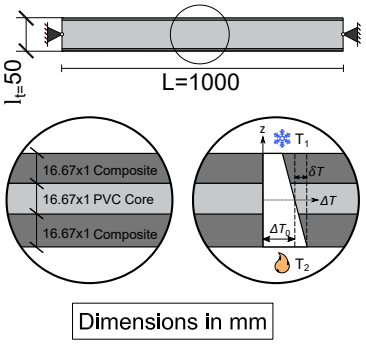

Figure 1: Description of the one-dimensional buckling problem.

In this example the difference between the hot and cold ends (δT) is of 1 °C and the thermal properties of the composite and the core is considered uniform and equal for sake of simplicity. The computational model of the domain described in Figure 1 consist of a plate that is simply supported on the upper and lower edge, the plate is discretised in 20×20 divisions of symmetric-structured triangles and the thickness is subdivided in 30 layers.

The expression of the critical load for a symmetrical cross-sectional composite simply supported beam can be written as

$$P_{cr} = \frac{\pi^2 D_b}{L^2} \tag{19}$$

where P_{cr} is the critical buckling load, L the length between supports and D_b is the bending component of the constitutive matrix, also referred as flexural rigidity

$$D_b = \int_{l_t} \left(Ez^2\right) \mathrm{d}z \tag{20}$$

The critical buckling load is equal to the axial force caused by the thermal expansion and can be written as

$$P_{cr} = -l_b \alpha \Delta T_0 \bar{E} \tag{21}$$

where l_b is the width of the beam, ΔT_0 is the increment of mean temperature and $\bar{E}$ is the axial rigidity (same concept as Equation 20 but without the inertia). Using Equation 19 and Equation 21, the critical increment of mean temperature is determined to be approximately 300 °C, however a higher load of 400 °C is introduced instead to proof the correctness of the corotational formulation.

Figure 2 show the correctness of the corotational theory in order to predict buckling. In the figure the solution for a linear-geometric DKT element is compared against the same element with the corotational formulation, the linear geometric converges to the analytical force for a temperature of 400 °C, whereas the non-linear geometric (corotational) stagnates when the time reaches the critical buckling temperature of 300 °C as it is supposed to happen. This is a clear proof on how the non-linear geometric theory predicts well the non-linear geometric stiffness in Equation 5.

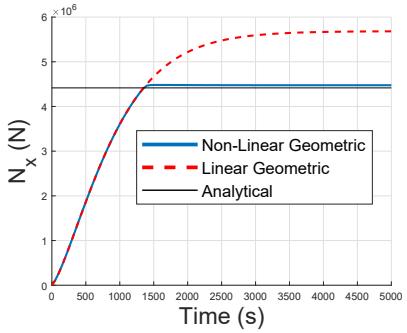

Figure 2: Elastic.

In Figure 2, the solution of the critical load is shown for elastic, degraded, inelastic thermal buckling and the combination of degraded and inelastic thermal buckling.

In Equation 19, the critical load obtained when the Young's modulus (E) is degraded to half would result in the half of the virgin critical load. Using a law such as Equation 13, the young modulus can be dependent on the temperature, assuming that near the critical temperature of 300 °C the elastic modulus is half of the virgin value, the numerical results in Figure 3 show a perfect agreement with the analytical buckling force and it can be observed that the critical buckling load has reduced to half. In real applications, materials even reduced more than half and that is why thermal buckling is a very important problem since it may lead to a prompt collapse of structural reinforcements in ships.

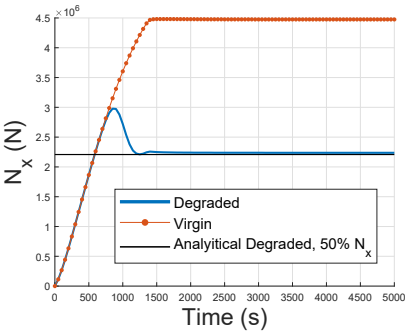

Figure 3: Degraded.

Generally, pure buckling is very uncommon in real life, inelastic buckling is easier to be observed. Inelastic buckling happens when a load-bearing member buckles and its own deflection generates fluency of the material that leads to damage, plasticity or fracture. In Figure 4, the Young's modulus is non-dependent of the temperature and instead the yield stress is reduced using Equation 13, both matrix and fibre have the same evolution respect temperature for the sake of simplicity. Observe that at the beginning, the inelastic and elastic numerical models match exactly, but as the yielding limit is reduced on both matrix and fibre, the fluency norm described in Equation 14 increases quicker since the yielding stress is lower and this accelerates the damage evolution of the fibre and matrix.

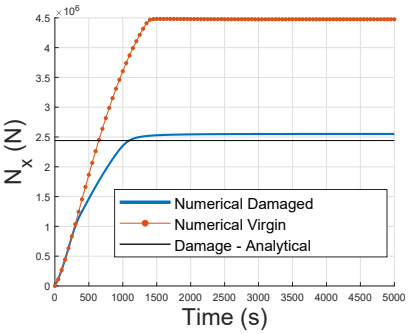

Figure 4: Inelastic.

At the end of the analysis the axial load converges to a lower load than the expected for the virgin material. This can be understood as if the Young's Modulus involved in the critical load is multiplied by $(1-d)$ where d is the damage index, this theoretical limit is shown in Figure 4. It is fundamental to understand that the design buckling load that a structural member can endure is reduced in inelastic buckling, however in the presence of thermal inelastic buckling, the result will be even worse since the yield stress is also reduced. It is interesting to note that this is directly related to the yield stress over Young's modulus ratio $(\frac{\sigma_y}{E})$ and how this evolves with respect to the temperature.

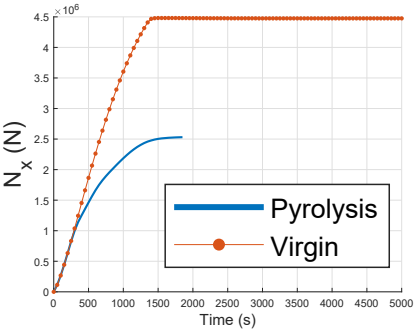

Figure 5: Pyrolysed and inelastic.

Figure 5 shows the outcome if pyrolysis is taken into account. The material considers pyrolysis and inelasticity but not thermal degradation of the mechanical properties as in Figure 3. The result seems similar to the inelastic case in Figure 4, nevertheless, when the mean pyrolysis parameter (F) is close to 0%, the beam collapses suddenly. This is in correspondence with Figure 6 that shows that near the time of collapse the pyrolysis process has a degradation fraction (F) close to zero, making the problem ill-conditioned as according to Equation 13, the Young's modulus tends to zero as well.

This evidences how critical is pyrolysis in the collapse of composite structures and in particular for buckling since the inelastic case could still endure a reduced load, whereas the inelastic pyrolysed case collapses dramatically.

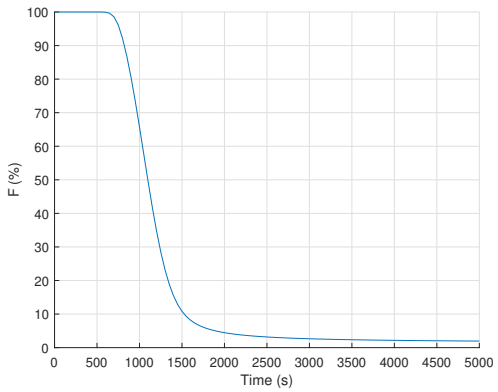

Figure 6: Evolution of the mean degradation of the section.

4.2 Laminate-plate buckling

The Laminate-plate buckling is a well known problem studied in (Al-Waily, 2015; Ounis et al., 2014; Shiau et al., 2010; Thangaratnam et al., 1989). This benchmark case shows the buckling phenomenon of orthotropic shells. The dimensions of this example can be found in Figure 7. The material is a symmetric monolithic composite stack of ten layers of uni-directional glass fibre and vinylester with a fibre volumetric fraction of 60%. The thermal properties of the fibre and matrix are considered the same as the composite. The mesh generated in this example is the same as in the Euler-buckling beam, but it is simply supported on all edges.

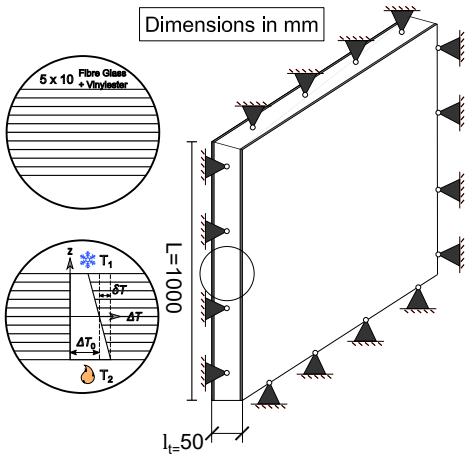

Figure 7: Description of the two-dimensional buckling problem.

The critical buckling temperature for different fibre orientations is compared against the analytical orthotropic solution. Fibre angle orientation is defined as follows, a 0°fibre orientation is aligned to the horizontal axis and 90°to the vertical axis. The height of the plate is 1000 mm and the width is variable, considering a total of 3 different width over height aspect ratios $(0.75, 1, 2)$. The minimum critical buckling temperature is then found (the ambient and initial temperatures are considered 0 °C) for these different aspect ratios. Similarly to (Al-Waily, 2015), the orthotropic definition of the critical buckling increment of temperature can be derived from plate theory for simply supported plates. Using the definition of the elastic constitutive matrix ($\mathbb{C}$) in Equation 12 and defining the plate flexural rigidity matrix (D) and the thermal buckling coefficient (η), the critical buckling increment of temperature yields

$$D = \int_{l_t} \mathbb{C} \cdot \begin{bmatrix} -z & 0 & 0 \\ 0 & -z & 0 \\ 0 & 0 & -4z \end{bmatrix} \cdot z \mathrm{d}z \qquad (22) \qquad \eta = \int_{l_t} \mathbb{C} \cdot \alpha \, \mathrm{d}z \qquad (23)$$

$$\Delta T_{\mathrm{cr}} = \frac{D_{11}\bar{a}^4 + \bar{a}^2\bar{b}^2(D_{12} + D_{21} + 2D_{33}) + D_{22}\bar{b}^4}{\eta_1\bar{a}^2 + \eta_2\bar{b}^2} \qquad (24)$$

where $\bar{a} = \frac{\pi n}{W}$ and $\bar{b} = \frac{\pi m}{L}$, W is the width of the plate, L is the length of the plate, n and m are the horizontal and vertical modes (the most critical ones are when $n = m = 1$).

Figure 8 shows the numerical results for the critical buckling mean temperature for different angles against the analytical orthotropic result obtained from Equation 24. It shows a very good agreement for aspect ratios of 0.75, 1 and 2. Note that in this example, the constitutive model is considered without pyrolysis and elastic as well, in contraposition to the Euler-buckling beam example. The SPROM theory demonstrates to correctly predict the two-dimensional thermal buckling of the plate, guaranteeing the correct prediction of buckling in laminate structures and also the possibility of adding thermal degradation (pyrolysis) and inelastic buckling as shown in the Euler-buckling example.

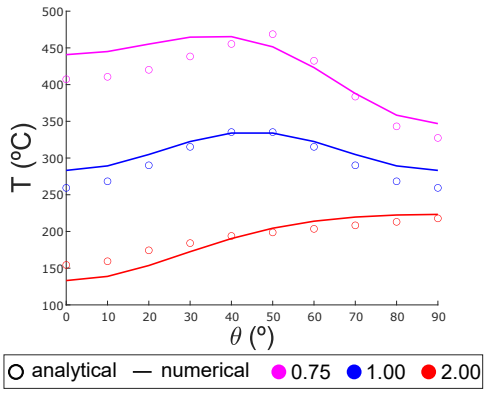

Figure 8: Critical temperature at different angles.

4.3 Thermal-buckling collapse of a container-ship

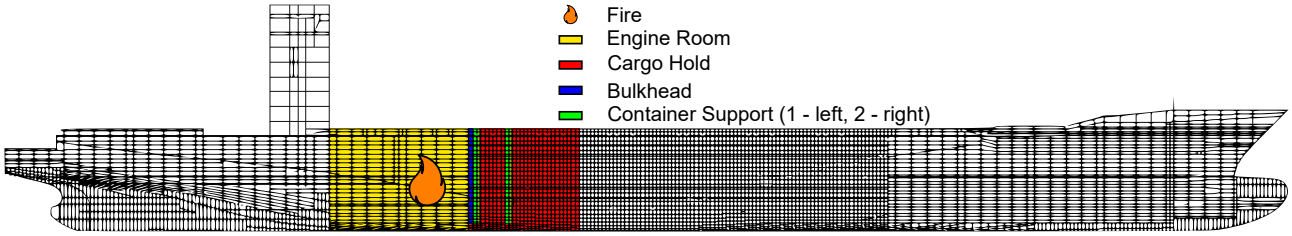

Figure 9: Container-ship profile section.

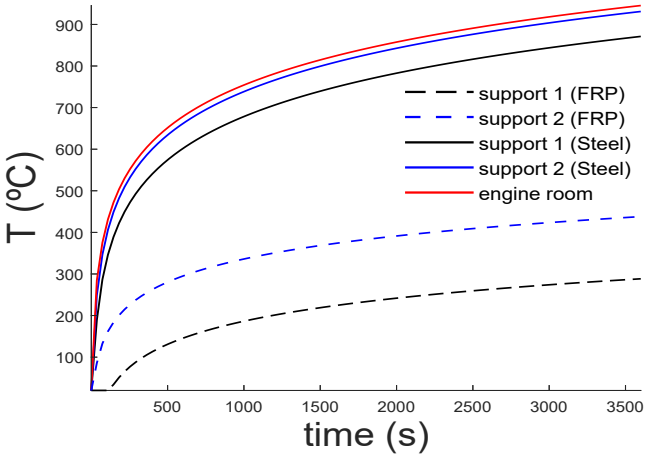

Figure 10: Thermal load for both steel and FRP design.

The containership design used in this example was generated from the research related to FIBRESHIP. It is assumed that in the engine room of the ship a fire is originated, the thermal load is then applied to the bulkhead between the engine room and the immediate cargo hold and it affects the two supports holding the TEU containers. The thermal load is assumed to be an ISO-834 during one hour of simulation. The adiabatic temperature prescribed is assumed to be those in Figure 10, unless thermal insulation is considered, then ambient temperature is considered instead (20 °C). Steel and FRP – standard glass fibre and epoxy resin – materials are considered for these structural members and also if the bulkhead was insulated from the side of fire.

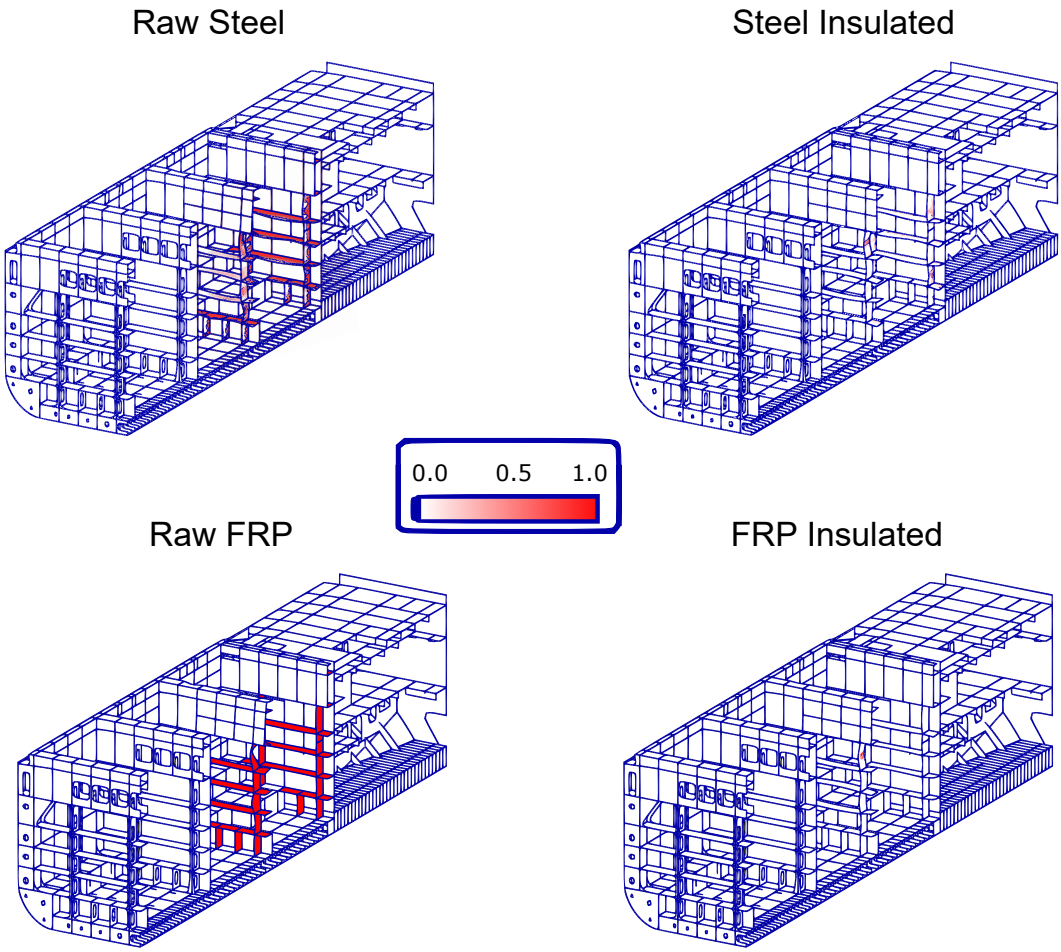

Figure 11: Damage and deformation of the structure for different designs.

In Figure 11 the four designs are shown. The raw steel without insulation shows that support 1 (the one closest to the bow) buckles at time 620s and there is significant damage in the supports before total collapse. When insulated there is a little damage on the vertical members of the support due to support 1 entering a post-buckling state, however the structure does not collapse and holds for 3600s. In the case of FRP without insulation, the structure suffers a higher damage even in the bulkhead since the material pyrolysis to relative low temperatures (200°C) and the structures collapses at 590s. If the FRP is insulated, the structure does not collapse and there is only one vertical structural member of support 1 that enters into post-buckling and presents damage.

5 CONCLUSIONS

In this paper a thermo-mechanical composite model was proposed to analyse non-linear geometric problems such buckling. It is clear that the euler-buckling beam problem showed that the corrotational formulation is able to predict buckling (Figure 2) and the effect of fire on the constitutive properties in order to take into account thermal degradation of mechanical properties (Figure 3 and Figure 4) and also the pyrolysis effect present in composites (Figure 5). The correctness to use the SPROM theory to model composites was shown in the laminate-buckling plate example since it was able to correctly predict 2D buckling for different aspect ratios and fibre orientations (Figure 8).

Finally a naval example was presented where a containership's structural response is analysed in the presence of fire. The developed methodology shows that it is possible to address the problem of thermal

buckling and post-buckling. Steel shows worse response if compared to composite. Composites degrade at temperatures lower than steel and despite so the difference of time when non-insulated is 590s for FRP and 620s for steel, despite steel having a glass temperature transition of 4 times greater than the glass-epoxy. This is due to the effect of higher conductivity in metal materials and the fact that composites pyrolyse.

Interestingly if the bulkhead is insulated the steel design obtains a worse result since various structural members of the supports enter in post-inelastic-buckling regime, this is because the bulkhead with insulation experiments a 10°C thermal gradient, causing it to endure less load and to redistribute it to the supports. The composite with insulation still shows that one structural member in support 1 has entered post-inelastic-buckling due to similar process as in steel.

Recall that the FRP configuration fulfils the concept of '*steel equivalent*' imposed by SOLAS and this evidences the efficiency of using composite materials in the design of marine structures. However, to use composites as design materials, which are naturally more flexible (prone to buckling), means to use methodologies as the ones shown in this paper, specially when fire is a major risk to take into account.

6 ACKNOWLEDGEMENT

This work was funded thanks to H2020 project FIBRESHIP sponsored by the EUROPEAN COMMISSION under the grant agreement 723360 "Engineering, production and life-cycle management for complete construction of large-length FIBRE-based SHIPs". www.fibreship.eu/about

Also to acknowledge the scantled model of the container-ship provided by Daniel Sá and Manuel López.

REFERENCES

Report on the Effects of Fire on LNG Carrier Containment Systems | SIGTTO - The Society of International Gas Tanker and Terminal Operators. Technical report, SIGTTO, 2009. URL `https://www.sigtto.org/publications/report-on-the-effects-of-fire-on-lng-carrier-containment-systems/`.

Abdoun, F., Azrar, L., Daya, E. M., and Rabat, I. Thermal buckling and post-buckling of laminated composite plates with temperature dependent properties by an asymptotic numerical method. Technical report.

Al-Waily, M. INTERNATIONAL JOURNAL OF ENERGY AND ENVIRONMENT Analytical and numerical thermal buckling analysis investigation of unidirectional and woven reinforcement composite plate structural. Technical Report 2, 2015. URL `www.IJEE.IEEFoundation.org`.

Asaro, R. J., Lattimer, B., and Ramroth, W. (2009). Structural response of FRP composites during fire. *Composite Structures*, 87(4):382–393. ISSN 02638223. doi: 10.1016/j.compstruct.2008.02.018. URL `https://linkinghub.elsevier.com/retrieve/pii/S0263822308000482`.

Car, E., Oller, S., and Oñate, E. (2000). An anisotropic elastoplastic constitutive model for large strain analysis of fiber reinforced composite materials. *Computer Methods in Applied Mechanics and Engineering*, 185(2-4):245–277. ISSN 00457825. doi: 10.1016/S0045-7825(99)00262-5.

Chaves, E. W. V. *Notes on Continuum Mechanics*. Lecture Notes on Numerical Methods in Engineering and Sciences. Springer Netherlands, Dordrecht, 2013. ISBN 978-94-007-5985-5. doi: 10.1007/978-94-007-5986-2. URL `http://link.springer.com/10.1007/978-94-007-5986-2`.

Chippendale, R. D., Golosnoy, I. O., and Lewin, P. L. (2014). Numerical modelling of thermal decomposition processes and associated damage in carbon fibre composites. *Journal of Physics D: Applied Physics*, 47(38):385301. ISSN 13616463. doi: 10.1088/0022-3727/47/38/385301. URL http://stacks.iop.org/0022-3727/47/i=38/a=385301http://stacks.iop.org/0022-3727/47/i=38/a=385301?key=crossref.e8e3fa511892bfff723543822db41f64.

Dhatt, G. S. (1970). An efficient triangular shell element. *AIAA Journal*, 8(11):2100–2102. ISSN 00011452. doi: 10.2514/3.6068.

Dodds, N., Gibson, A. G., Dewhurst, D., and Davies, J. M. (2000). Fire behaviour of composite laminates. *Composites Part A: Applied Science and Manufacturing*, 31(7):689–702. ISSN 1359835X. doi: 10.1016/S1359-835X(00)00015-4.

Felippa, C. A. (2003). A study of optimal membrane triangles with drilling freedoms. *Computer Methods in Applied Mechanics and Engineering*, 192(16-18):2125–2168. ISSN 00457825. doi: 10.1016/S0045-7825(03)00253-6.

Felippa, C. A. and Haugen, B. (2005). A unified formulation of small-strain corotational finite elements: I. Theory. *Computer Methods in Applied Mechanics and Engineering*, 194(21-24 SPEC. ISS.):2285–2335. ISSN 00457825. doi: 10.1016/j.cma.2004.07.035.

Gibson, A. G., Wu, Y. S., Chandler, H. W., Wilcox, J. A. D., and Bettess, P. (1995). A Model for the Thermal Performance of Thick Composite Laminates in Hydrocarbon Fires. *Revue de l'Institut Français du Pétrole*, 50(1):69–74. ISSN 0020-2274. doi: 10.2516/ogst:1995007. URL http://ogst.ifpenergiesnouvelles.fr/10.2516/ogst:1995007.

Gibson, A. G., Wright, P. N. H., Wu, Y. S., Mouritz, A. P., Mathys, Z., and Gardiner, C. P. (2004). The Integrity of Polymer Composites during and after Fire. *Journal of Composite Materials*, 38(15):1283–1307. ISSN 0021-9983. doi: 10.1177/0021998304042733. URL http://journals.sagepub.com/doi/10.1177/0021998304042733.

Green, A. E. and Naghdi, P. M. (1965). A Dynamical theory of interacting continua. *International Journal of Engineering Science*, 3(2):231–241. ISSN 00207225. doi: 10.1016/0020-7225(65)90046-7.

Henderson, J. and Wiecek, T. (1987). A Mathematical Model to Predict the Thermal Response of Decomposing, Expanding Polymer Composites. *Journal of Composite Materials*, 21(4):373–393. ISSN 0021-9983. doi: 10.1177/002199838702100406. URL http://journals.sagepub.com/doi/10.1177/002199838702100406.

Henderson, J., Wiebelt, J., and Tant, M. (1985). A Model for the Thermal Response of Polymer Composite Materials with Experimental Verification. *Journal of Composite Materials*, 19(6):579–595. ISSN 0021-9983. doi: 10.1177/002199838501900608. URL http://journals.sagepub.com/doi/10.1177/002199838501900608.

Holmas, T. and Amdahl, J. Advanced structural fire design of offshore structures. Technical report.

Looyeh, M. R. and Bettess, P. (1998). A finite element model for the fire-performance of GRP panels including variable thermal properties. *Finite Elements in Analysis and Design*, 30(4):313–324. ISSN 0168874X. doi: 10.1016/S0168-874X(98)00036-5.

Lua, J., O'Brien, J., Key, C. T., Wu, Y., and Lattimer, B. Y. (2006). A temperature and mass dependent thermal model for fire response prediction of marine composites. *Composites Part A: Applied Science and Manufacturing*, 37(7):1024–1039. ISSN 1359835X. doi: 10.1016/j.compositesa.2005.01.034.

Mouritz, A. P. and Gibson, A. G. *Fire Properties of Polymer Composite Materials*, volume 143 of *Solid Mechanics and Its Applications*. Springer Netherlands, Dordrecht, 2006. ISBN 978-1-4020-5355-9. doi: 10.1007/978-1-4020-5356-6. URL http://link.springer.com/10.1007/978-1-4020-5356-6.

Mouritz, A. P. and Mathys, Z. (2000). Mechanical properties of fire-damaged glass-reinforced phenolic composites. *Fire and Materials*, 24(2):67–75. ISSN 1099-1018. doi: 10.1002/1099-1018(200003/04)24:2<67::AID-FAM720>3.0.CO;2-0.

Mouritz, A. P. and Mathys, Z. (2001). Post-fire mechanical properties of glass-reinforced polyester composites. *Composites Science and Technology*, 61(4):475–490. ISSN 02663538. doi: 10.1016/S0266-3538(00)00204-9.

Mouritz, A. P., Feih, S., Kandare, E., Mathys, Z., Gibson, A. G., Des Jardin, P. E., Case, S. W., and Lattimer, B. Y. (2009). Review of fire structural modelling of polymer composites. *Composites Part A: Applied Science and Manufacturing*, 40(12):1800–1814. ISSN 1359835X. doi: 10.1016/j.compositesa.2009.09.001. URL http://dx.doi.org/10.1016/j.compositesa.2009.09.001.

Oñate, E. Structural Analysis with the Finite Element Method Linear Statics Volume 2. Beams, Plates and Shells. In *Springer*, volume First Edit, chapter 11, pages 675–728. 2013. ISBN 9781402087325. doi: 10.1007/978-1-4020-8743-1. URL http://medcontent.metapress.com/index/A65RM03P4874243N.pdf.

Ounis, H., Tati, A., and Benchabane, A. (2014). Thermal buckling behavior of laminated composite plates: A finite-element study. *Frontiers of Mechanical Engineering*, 9(1):41–49. ISSN 20950241. doi: 10.1007/s11465-014-0284-z. URL https://link.springer.com/article/10.1007/s11465-014-0284-z.

Rastellini, F., Oller, S., Salomón, O., and Oñate, E. (2008). Composite materials non-linear modelling for long fibre-reinforced laminates. *Computers & Structures*, 86(9):879–896. ISSN 00457949. doi: 10.1016/j.compstruc.2007.04.009. URL https://linkinghub.elsevier.com/retrieve/pii/S0045794907001642.

Reuss, A. (1929). Berechnung der Fließgrenze von Mischkristallen auf Grund der Plastizitätsbedingung für Einkristalle . *ZAMM - Journal of Applied Mathematics and Mechanics / Zeitschrift für Angewandte Mathematik und Mechanik*, 9(1):49–58. ISSN 15214001. doi: 10.1002/zamm.19290090104. URL http://doi.wiley.com/10.1002/zamm.19290090104.

Shakir Abbood, I., Odaa, S. a., Hasan, K. F., and Jasim, M. A. (2020). Properties evaluation of fiber reinforced polymers and their constituent materials used in structures – A review. *Materials Today: Proceedings*. ISSN 22147853. doi: 10.1016/j.matpr.2020.07.636. URL https://linkinghub.elsevier.com/retrieve/pii/S2214785320357618.

Shiau, L. C., Kuo, S. Y., and Chen, C. Y. (2010). Thermal buckling behavior of composite laminated plates. *Composite Structures*, 92(2):508–514. ISSN 02638223. doi: 10.1016/j.compstruct.2009.08.035. URL https://linkinghub.elsevier.com/retrieve/pii/S0263822309003146.

Thangaratnam, K. R., Palaninathan, and Ramachandran, J. (1989). Thermal buckling of composite laminated plates. *Computers and Structures*, 32(5):1117–1124. ISSN 00457949. doi: 10.1016/0045-7949(89)90413-6. URL https://linkinghub.elsevier.com/retrieve/pii/0045794989904136.

Tran, P., Nguyen, Q. T., and Lau, K. T. Fire performance of polymer-based composites for maritime infrastructure, 12 2018. ISSN 13598368. URL https://linkinghub.elsevier.com/retrieve/pii/S1359836818315968.

Voigt, W. (1889). Ueber die Beziehung zwischen den beiden Elasticitätsconstanten isotroper Körper. *Annalen der Physik*, 274(12):573–587. ISSN 15213889. doi: 10.1002/andp.18892741206. URL http://onlinelibrary.wiley.com/doi/10.1002/andp.18892741206/abstract.

Wickstrom Ulf, S. N., Duthinh, D., and Mcgrattan, K. (2007). Adiabatic Surface Temperature for Calculating Heat Transfer To Fire Introduction. *Most*, 2. URL https://www.nist.gov/publications/adiabatic-surface-temperature-calculating-heat-transfer-fire-exposed-structures.